Upstream Ionization Instability Associated with a Current-Free Double Layer

A. Aanesland,* C. Charles, M. A. Lieberman,† and R. W. Boswell

SP3, Research School of Physical Sciences and Engineering, The Australian National University, Australian Capital Territory 0200, Australia

(Received 5 June 2006; published 18 August 2006)

A low frequency instability has been observed using various electrostatic probes in a low-pressure expanding helicon plasma. The instability is associated with the presence of a current-free double layer (DL). The frequency of the instability increases linearly with the potential drop of the DL, and simultaneous measurements show their coexistence. A theory for an upstream ionization instability has been developed, which shows that electrons accelerated through the DL increase the ionization upstream and are responsible for the observed instability. The theory is in good agreement with the experimental results.

DOI: 10.1103/PhysRevLett.97.075003 PACS numbers: 52.35.−g

Double layers (DLs) are spatially isolated, rapid changes of potential in a plasma and are important structures for accelerating charged particles. A well-known example is the acceleration of the aurora electrons [1], and recently, it has been suggested that DLs are also responsible for the acceleration mechanism in corona funnels [2]. Current-free electric double layers (CFDLs) have received considerable attention for the last several years [3–7]. CFDLs spontaneously form in expanding low-pressure plasmas; they are stable in space and time and they form within the first 100 μs of the breakdown [8]. There is no evidence of abrupt unstable behaviors, and the DL does not propagate. Ion energy distribution functions (IEDF) measured with a retarding field energy analyzer (RFEA) have shown the presence of a supersonic ion beam downstream of the DL [4]. A recently developed theory for the formation of CFDLs incorporates, in addition to the downstream ion beam, an electron beam upstream of the DL at the high potential side which enhances the ionization in this region [9]. Preliminary experimental results have shown evidence supporting the presence of this electron beam [4].

The first measurements of low frequency instabilities that are associated with the CFDL are presented here. We interpret them as an upstream ionization instability [10–12] resulting from the additional ionization caused by the energized electron beam. A theory of the instability is developed, based on [9,10]. Both the theory and the experiment show that the frequency of the instability increases linearly with the potential drop of the DL.

The experiments are performed in the helicon source Chi-Kung, where CFDLs have been previously investigated [3,4]. The plasma is created by a helicon-type antenna powered at 13.56 MHz, which is wrapped around a cylindrical insulating source chamber. The source is connected to a larger diameter grounded diffusion chamber, and the plasma is allowed to expand due to the geometrical expansion as well as a diverging magnetic field. The CFDL forms spontaneously in the source a short distance from the junction with the diffusion chamber for pressures between 0.2 and 2 mTorr in argon [9].

A Langmuir probe (LP) is used to measure the fluctuations of the floating potential V_f (probe floating into 1 MΩ), the ion saturation current $V_{i,\mathrm{sat}}$ (probe biased at −56 V), and the electron saturation current $V_{e,\mathrm{sat}}$ (probe biased at +56 V). An emissive probe is used to measure the fluctuations directly on the plasma potential V_p (by applying a heating current the floating probe sits at the plasma potential). An RFEA measuring the IEDF downstream is used together with the LP to simultaneously measure the presence of the DL (i.e., the presence of a downstream ion beam) and the instability. Additionally the RFEA allows us to measure the fluctuations on the beam ion current I_{beam} directly, acquiring the frequency spectrum at different discriminator voltages.

The frequency spectrum is measured over a broad frequency range from 1 to 30 MHz. We emphasize here the fluctuations observed at 5–20 kHz, which are present only when the CFDL exists. A typical spectrum from 0 to 30 kHz is inset in Fig. 1 and shows a pronounced peak at ∼15 kHz.

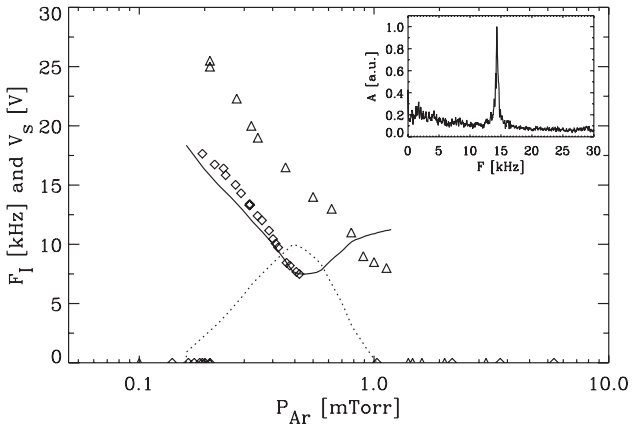

FIG. 1. Frequency of instability (diamonds) and potential drop of the double layer (triangles) as a function of pressure. Inset is a normalized spectrum at 0.3 mTorr; the solid line shows the theoretical calculation of frequency for a wave number $k_0 = 26\ \mathrm{m}^{-1}$, and the dotted line is the corresponding growth rate.

The instability frequency F_I and amplitude A_I have been measured as a function of pressure, magnetic field, rf power, and radial and axial position. In this Letter we present the measurements of V_f and I_{beam}; however, the instability is observed on all plasma parameters (V_f, $I_{i,\text{sat}}$, $I_{e,\text{sat}}$, V_p, I_{beam}) and are consistent with the ones presented here.

Figure 1 shows the measured frequency F_I and potential drop of the double layer V_s as a function of pressure and shows a linear dependency between F_I and V_s. The rf power is 250 W and the diverging magnetic field is 125 G in the source. The floating LP is on axis about 5 cm upstream ($r = 0$ cm, $z = 20$ cm), while the RFEA is about 12 cm downstream of the DL ($r = 0$ cm, $z = 37$ cm). The same variation of frequency with pressure has been measured on and off axis, upstream and downstream of the DL, with the LP floating or biased to ion saturation, and with the emissive probe. Simultaneous measurements confirm that the ion beam and the instability disappear at the same lower pressure threshold of 0.2 mTorr. The noise in the low frequency spectrum increases at pressures between 0.6 and 1 mTorr, and the frequency could not be measured accurately. However, we observed that the frequency seems to saturate at 5 kHz before it disappears at 2 mTorr, but the amplitude is small and almost into the noise. The data points are therefore not plotted at these pressures. The corresponding instability amplitude has a maximum at 0.3–0.4 mTorr. The plasma density upstream and downstream of the DL increases slowly, and the electron temperature decreases, as a function of increasing pressure in this range. Hence, A_I does not directly follow the plasma density evolution, but the axial and radial variation in A_I roughly follow the axial and radial variation in the density when no other parameters are changed (F_I remains constant).

Figure 2 shows the IEDF (solid line) at a pressure of 0.3 mTorr with a background cold ion population with an energy corresponding to the plasma potential of 26 V and an ion beam at an energy peak of 53 V. At this downstream position the ion beam density, found by integrating the IEDF, is about 10% of the background ions. The low frequency spectrum is measured on the collector current of the RFEA while the discriminator voltage V_d is increased stepwise from 0 to 60 V; the measured instability amplitude is shown by the diamonds in Fig. 2 (F_I being constant at 15 kHz). When $V_d = 0$ V all of the ions contribute to the measured collector current, while when $V_d = 47$ V only the beam ions can reach the collector, i.e., only 10% of the ions. Interestingly, A_I drops only 50% at $V_d = 47$ V and remains constant until no ions can enter the RFEA at 60 V. Rotating the RFEA perpendicular to the ion beam allows one to measure the population of cold background ions only [4]. In this case A_I drops by as much as 70% at $V_d = 0$ V (compared to the RFEA facing the DL). Hence, it seems that the ion beam downstream is strongly influenced by the instability, and we therefore suspect that the instability is "born" upstream and carried by the ion beam downstream of the DL.

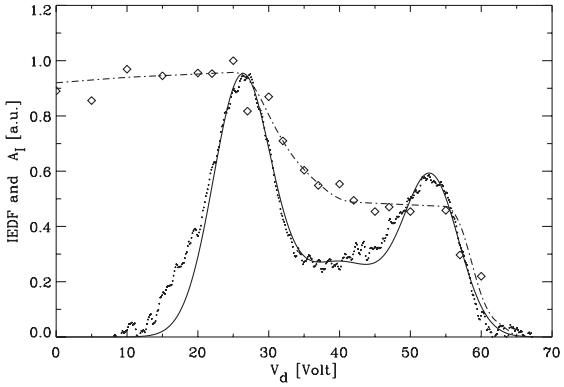

FIG. 2. Normalized ion energy distribution function (data points and solid line), and the corresponding normalized amplitude of the 15 kHz instability measured on the collector as a function of the discriminator voltage (diamonds and dash-dotted line).

Johnson *et al.* [10] observed low frequency instabilities in their double plasma device when current-driven DLs were present, and they suggested that electrons accelerated by the DL potential drop may excite an ionization instability in the upstream region. As the ionization collision cross section is a rapidly increasing function of the electron energy (close to the ionization threshold), the beam electrons will add to the ionization in the upstream region. The underlying assumption for this instability to grow is the existence of some electrostatic perturbation in the plasma; the ionization rate will then be higher at the wave crest, increasing the amplitude of the potential fluctuations. In the one-dimensional fluid model of Johnson *et al.* a monoenergetic beam of electrons with energy slightly higher than the ionization energy was assumed to account for all the ionization in the upstream region, and the ionization by the Maxwellian population of background electrons was neglected. This model was later modified to account for the contribution from the cold electron population in addition to assuming a nonquasineutral perturbation [11]. The model has also been adapted to dusty plasmas, where negatively charged dust grains have been taken into account [12].

The theoretical analysis presented here includes an accelerated non-Maxwellian group of electrons upstream, due to the flow of downstream electrons, created by electron-neutral ionization, across the double layer. A two-dimensional low-pressure diffusion analysis is used. The plasma equilibrium, with uniform particle densities in the bulk that drop relatively sharply at the plasma-sheath edge, is found in the upstream region by balancing the creation and loss of ions, yielding

$$n_d n_g K_{\text{iz}} + n_c n_g K_{\text{iz}c} - \nu_L n_i = 0, \tag{1}$$

where n_d is the thermal electron density, n_g is the neutral

gas density, $K_{iz}(T_e)$ is the thermal electron-neutral ionization rate coefficient, n_c is the accelerated (beam) electron density, $K_{izc}(V_s, T_e)$ is the accelerated electron-neutral ionization rate coefficient,

$$\nu_L = \left(\frac{2h_l}{l} + \frac{2h_R}{R}\right)u_B \tag{2}$$

is the upstream particle loss frequency, $n_i = n_d + n_c$ is the ion density, T_e is the common thermal electron temperature in the upstream and downstream regions, and $u_B = (eT_e/M)^{1/2}$ is the Bohm velocity, with M the ion mass. In (2) we assume no reduction in the radial losses due to the upstream magnetic field, and $h_l = 0.86/(3 + l/2\lambda_i)^{1/2}$ and $h_r = 0.8/(4 + R/\lambda_i)^{1/2}$ are the axial and radial edge-to-center density ratios [9,13], with l and R the length and radius of the upstream region and λ_i the (constant) ion-neutral mean free path. The ionization rate coefficient K_{izc} for the upstream accelerated electrons was calculated in [9] and depends on both V_s and T_e. The second term in (1) corresponds to the energy dependent cross section used in [10,11] but accounts for the non-Maxwellian distribution of the electron beam rather than assuming a monoenergetic beam.

Assuming that the perturbed quantities vary as $\exp(j\omega t - jkz)$, the perturbed ion balance/continuity relation is

$$j\omega\tilde{n}_i + n_i\nabla\cdot\tilde{v}_i = \tilde{n}_d n_g K_{iz} + \tilde{n}_c n_g K_{izc} + n_c n_g K'_{izc}\tilde{\varphi} - \nu_L\tilde{n}_i, \tag{3}$$

where the tildes denote the perturbed quantities. $\tilde{K}_{izc} \simeq K'_{izc}\tilde{\varphi}$ by a first order approximation, where $K'_{izc} = \partial K_{izc}/\partial V_s$ and $\tilde{\varphi}$ is the perturbed potential in the plasma. Differentiating K_{izc}, from [9], with respect to V_s, gives the results for K'_{izc} vs V_s plotted in Fig. 3 for various values of T_e.

To solve for the wave dispersion, the perturbed quantities ($\tilde{v}_i$, $\tilde{n}_d$, $\tilde{n}_c$, and $\tilde{n}_i$) are found as a function of $\tilde{\varphi}$, which allows us to express (3) solely by the perturbed potential. The perturbed ion velocity $\tilde{v}_i$ is found from the first order ion momentum relation

$$j\omega M\tilde{v}_i = -e\nabla\tilde{\varphi} - M\nu_{mi}\tilde{v}_i, \tag{4}$$

where $\nu_{mi} = u_i/\lambda_i$ is the ion-neutral momentum transfer frequency, with u_i the mean ion speed. For $R \ll l$ in the low-pressure regime $T_i/T_e \ll \lambda_i/R \ll 1$, u_i can be best fitted as $u_i \approx u_B h_R$, such that

$$\nu_{mi} \approx h_R u_B/\lambda_i. \tag{5}$$

The linear relation between the thermal electron perturbed density and the perturbed potential is found from the Boltzmann relation

$$\tilde{n}_d = n_d(e^{\tilde{\varphi}/T_e} - 1) \simeq n_d\frac{\tilde{\varphi}}{T_e}, \tag{6}$$

where the latter equality follows because $\tilde{\varphi} \ll T_e$. Since the upstream accelerated electrons have a non-Maxwellian (beamlike) axial velocity distribution [9], we can use the Vlasov equation

$$j\omega\tilde{f}_c - jk_z v_z\tilde{f}_c - jk_z\frac{e}{m}\frac{\partial f_c}{\partial v_z}\tilde{\varphi} = 0, \tag{7}$$

to determine the corresponding relation between $\tilde{n}_c$ and $\tilde{\varphi}$. Solving for the perturbed distribution function $\tilde{f}_c$ and integrating over velocity space determines the perturbed density of the beam electrons $\tilde{n}_c$. We use the conditions $\omega/k_z \ll v_s$ and $T_e \ll V_s$, which are well satisfied for the instability regime, to evaluate the integral, yielding

$$\tilde{n}_c = -n_c\frac{\tilde{\varphi}}{2V_s}. \tag{8}$$

Note that the signs in (6) and (8) are different, expressing the fact that thermal electrons gather into regions of higher potential, whereas the beam electron density decreases when the velocity increases, as the beam enters a region of higher potential. We assume a quasineutral perturbation $\tilde{n}_i = \tilde{n}_d + \tilde{n}_c$, where $\tilde{n}_d$ and $\tilde{n}_c$ are given by (6) and (8), respectively. Nonquasineutral perturbations were examined in [11] and yielded corrections of order $\lambda_D^2/R^2 \ll 1$, where λ_D is the Debye length.

Finally, substituting all the perturbed quantities into Eq. (3) gives the perturbed potential

$$j\omega\left(\frac{n_d}{T_e} - \frac{n_c}{2V_s}\right)\tilde{\varphi} - n_i\left(\frac{e}{M}\frac{1}{j\omega + \nu_{mi}}\right)\nabla^2\tilde{\varphi} = n_d\nu_{iz}\frac{\tilde{\varphi}}{T_e} - n_c\nu_{izc}\frac{\tilde{\varphi}}{2V_s} + n_c\Delta\nu_{izc}\frac{\tilde{\varphi}}{T_e} - \nu_L\left(\frac{n_d}{T_e} - \frac{n_c}{2V_s}\right)\tilde{\varphi}, \tag{9}$$

where $\nu_{iz} = n_g K_{iz}$, $\nu_{izc} = n_g K_{izc}$, and $\Delta\nu_{izc} = n_g K'_{izc} T_e$. The thermal electron ionization frequency ν_{iz} was determined in [9] to be consistent with the "downstream" particle loss rate

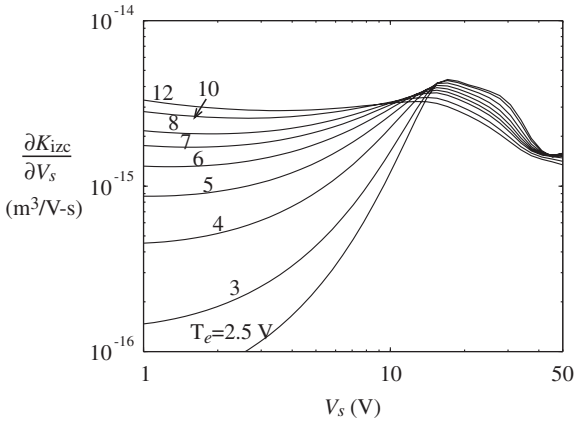

FIG. 3. Derivative $K'_{izc} = \partial K_{izc}/\partial V_s$ of the upstream beam ionization rate coefficient with respect to the double layer potential V_s vs V_s at various values of T_e.

$$\nu_{\mathrm{iz}} = \left(\frac{h_{l_1}}{l_1} + \frac{2h_{R_1}}{R_1}\right)u_B, \tag{10}$$

with h_{l_1} and h_{R_1} the downstream axial and radial edge-to-center density ratios, and l_1 and R_1 the downstream length and radius. Introducing the upstream accelerated electron fraction η, such that $n_c = \eta n_i$ and $n_d = (1-\eta)n_i$, and introducing the ratio $\epsilon = T_e/2V_s$, then (9) can be written in the form of a Helmholtz equation

$$\nabla^2\tilde{\varphi} + k^2\tilde{\varphi} = 0, \tag{11}$$

with the wave number k given by

$$k^2u_B^2 = (j\omega + \nu_{\mathrm{mi}})[(1+\epsilon)(1-\eta)(\nu_{\mathrm{iz}} - \nu_L) + \eta\Delta\nu_{\mathrm{izc}} - j\omega(1-\eta-\epsilon\eta)], \tag{12}$$

where ν_{izc} is eliminated using (1). Equation (12) is a quadratic equation for ω of the form $A\omega^2 + jB\omega - C = 0$, with the coefficients

$$\begin{aligned} A &= 1-\eta-\epsilon\eta, \\ B &= \eta\Delta\nu_{\mathrm{izc}} - \nu_{\mathrm{mi}}(1-\eta-\epsilon\eta) - (1-\eta)(1+\epsilon)(\nu_L - \nu_{\mathrm{iz}}), \\ C &= k^2u_B^2 + \nu_{\mathrm{mi}}(1-\eta)(1+\epsilon)(\nu_L - \nu_{\mathrm{iz}}) - \nu_{\mathrm{mi}}\eta\Delta\nu_{\mathrm{izc}}. \end{aligned} \tag{13}$$

Solving (12) yields the wave frequency for any given (real) wave number k. For $4AC - B^2 > 0$, the solution for ω has real and imaginary parts given by $\mathrm{Re}\omega = (4AC - B^2)^{1/2}/2A$ and $\mathrm{Im}\omega = -B/2A$. The wave is unstable for $\mathrm{Im}\omega < 0$; i.e., $B > 0$. For $4AC - B^2 < 0$, the wave has $\mathrm{Re}\omega = 0$ and is unstable for $B > 0$.

The coefficients A, B, and C given by (13) can be expressed in terms of the neutral pressure P_{Ar}, the double layer potential drop V_s, and the electron temperature T_e. Each pressure gives a set of V_s and T_e, where V_s is found experimentally using Fig. 1 and T_e is calculated theoretically using (11). This set is then used to determine the variation in frequency ($f = \mathrm{Re}\omega/2\pi$) as a function of pressure alone. To compare the theory with the experiments, we use $l = 31$ cm, $R = 6.85$ cm, $l_1 = 29.4$ cm, and $R_1 = 15.9$ cm, which gives $h_l = 0.43$, $h_R = 0.38$, $h_{l_1} = 0.39$, and $h_{R_1} = 0.36$. We use $\Delta\nu_{\mathrm{izc}} = n_g K'_{\mathrm{izc}} T_e$ and find numerically the values of K'_{izc} for the corresponding sets of (V_s, T_e) shown in Fig. 3.

The wave vector k in (11) is found, centering a cylindrical coordinate system on axis at the midplane of the upstream region, to be $\tilde{\varphi} = \tilde{\varphi}_0 \cos k_z z J_0(k_r r)$ with $k_z^2 + k_r^2 = k^2$. For boundary conditions such that $\tilde{\varphi} = 0$ at $z = \pm l/2$ and $\tilde{\varphi} = 0$ at $r = R$, we obtain k_z and k_r for the normal mode with the smallest eigenvalue k^2 given by $k_z = \pi/l$ and $k_r = \chi_{01}/R$, with $\chi_{01} \approx 2.405$ the first zero of the zero-order Bessel function J_0. From this we obtain $k = 37\ \mathrm{m}^{-1}$; however, using a somewhat smaller value, $k_0 = 26\ \mathrm{m}^{-1}$, fits better to the experimental results. The wave number is mainly determined by the radial variation of the perturbed potential and density given by k_r. In order to justify a somewhat reduced k_r, $\tilde{\varphi}$ and $\tilde{n}$ might not fall to zero at the chamber radius but at some larger effective radius instead. Using $r = 10$ cm rather than $r = 6.8$ cm gives $k = 26\ \mathrm{m}^{-1}$, as used in Fig. 1. The electron beam density previously determined [9] gives $\eta = 0.27$. Figure 1 shows the calculated (solid line) and measured (diamonds) frequency as a function of pressure. The dotted line is the normalized values ($\times 10$) of the growth rate, $\mathrm{Im}\omega$, which shows that the solution is unstable for the DL cases. A good correlation between the measured amplitude and the wave growth is observed. The system is stable in the absence of the accelerated electrons upstream. For this limit, the upstream equilibrium condition is $\nu_{\mathrm{iz}} = \nu_L$ with $\eta = 0$. Using these conditions in (13), we obtain $A = 1$, $B = -\nu_{\mathrm{mi}}$, and $C = k^2u_B^2$, representing a damped ion-acoustic mode in the upstream chamber. Note that the calculated frequency increases in the pressure range where the low frequency noise in the spectrum was too high for the instability to be detected experimentally (0.6–2 mTorr). The growth rate in this pressure range is, although positive, very small as seen by the dotted line in Fig. 1, which is consistent with the small amplitudes seen experimentally.

In summary, we have investigated a low frequency instability occurring in low-pressure plasmas only when a current-free double layer exists. The frequency of the instability increases as a function of the double layer potential drop. The experimental results are in good agreement with the presented theory of an ionization instability as a result of an electron beam being accelerated by the potential drop of the DL adding to the ionization in this region.

*Electronic address: ane.aanesland@anu.edu.au
†Permanent address: Department of Electrical Engineering and Computer Sciences, University of California, Berkeley, CA 94720, USA.

[1] L. Block, Astrophys. Space Sci. **55**, 59 (1978).
[2] R. W. Boswell, E. Marsch, and C. Charles, Astrophys. J. **640**, L199 (2006).
[3] C. Charles and R. Boswell, Appl. Phys. Lett. **82**, 1356 (2003).
[4] C. Charles and R. Boswell, Phys. Plasmas **11**, 1706 (2004).
[5] S. A. Cohen, N. Siefert, S. Stange, E. Scime, and F. Levinton, Phys. Plasmas **10**, 2593 (2003).
[6] X. Sun, A. M. Keesee, C. Biloiu, E. E. Scime, A. Meige, C. Charles, and R. W. Boswell, Phys. Rev. Lett. **95**, 025004 (2005).
[7] A. Meige, R. Boswell, C. Charles, and M. Turner, Phys. Plasmas **12**, 052317 (2005).
[8] C. Charles and R. Boswell, Phys. Plasmas **11**, 3808 (2004).
[9] M. A. Lieberman, C. Charles, and R. W. Boswell, J. Phys. D **39**, 3294 (2006).
[10] J. C. Johnson, N. D'Angelo, and R. L. Merlino, J. Phys. D **23**, 682 (1990).
[11] L. Conde, Phys. Plasmas **11**, 1955 (2004).
[12] N. D'Angelo, Phys. Plasmas **4**, 3422 (1997).
[13] M. A. Lieberman and A. J. Lichtenberg, *Principles of Plasma Discharges and Materials Processing* (Wiley-Interscience, New York, 2005), 2nd ed.